Programmable Assembly of Ground State Fermionic Tweezer Arrays

Naman Jain,[1] Jin Zhang,[1] Marcus Culemann,[1] and Philipp M. Preiss[1,2,*]
[1]Max Planck Institute of Quantum Optics, Hans-Kopfermann-Straße 1, Garching 85748, Germany
[2]Munich Center for Quantum Science and Technology (MCQST), Schellingstraße 4, München 80799, Germany

(Received 19 December 2025; accepted 6 April 2026; published 5 June 2026)

We demonstrate deterministic preparation of arbitrary two-component product states of fermionic ^{6}Li atoms in an 8×8 optical tweezer array, achieving motional ground-state fidelities above 98.5%. Leveraging the large differential magnetic moments for spin-resolution, with parallelized site- and number-resolved control, our approach addresses key challenges for low-entropy quantum state engineering. Combined with high-fidelity spin-, site-, and density-resolved readout within a single 20 μs exposure, and 3 s experimental cycles, these advances establish a fast, scalable, and programmable architecture for fermionic quantum simulation.

DOI: 10.1103/fsmh-dz71

Exercising precise control over microscopic quantum systems is a central theme in modern physics, underpinning advances across quantum simulation, information science, and metrology [1–3]. Neutral atom platforms provide a powerful approach to this endeavor, as demonstrated by rapid progress in their deterministic initialization and high-fidelity detection [4–6]. While fast single-atom preparation in optical tweezers via light-assisted collisions has enabled defect-free assembly of atomic arrays [7–9], initializing many atoms into a single programmable quantum state remains an experimental challenge. Achieving full control over internal and external degrees of freedom is particularly important for fermions, where strongly correlated Hubbard physics arises from the interplay between spin and charge correlations [10,11]. Arbitrary experimental control over many fermionic atoms at the level of single quantum states would allow the assembly of such Hubbard systems, with interesting applications in the study of out-of-equilibrium entanglement dynamics, spin transport, and quantum thermalization [12–14].

Fermionic quantum simulators based on quantum gas microscopes have uncovered rich itinerant many-body physics, including antiferromagnetic correlations, quasiparticle dynamics, and pseudogap signatures—through a top-down approach using bulk loading into optical lattices [15–17]. In practice, this requires sophisticated cooling and entropy redistribution schemes, which restrict the accessible configurations and often result in experimental cycle times of tens of seconds [18]. Complementary bottom-up approaches using few-fermion preparation in tweezers have enabled studies of quantum statistics, Laughlin states, and tunnel-coupled arrays up to eight sites [19–21]. These successes motivate architectures that merge the strengths of both approaches [22], realizing high repetition rates, low-entropy initialization with local spin control, and high-fidelity readout.

Here, we demonstrate such an approach by assembling and detecting 2D fermionic atom arrays with arbitrary density and spin distributions (Fig. 1), achieving complete control over the relevant internal and motional degrees of freedom within 3 s cycle times. This level of control emerges from several advances developed in this Letter. We establish a robust loading protocol that draws degenerate Fermi samples from a cold reservoir into a tweezer array without being limited by reservoir size. Local evaporation in the tweezers enables deterministic preparation of singlet pairs in the 3D motional ground state of each trap, as first demonstrated in [10]. To achieve site-resolved spin control in ^{6}Li, we exploit the Zeeman structure to tune the differential magnetic moment between the two lowest hyperfine states, and combine it with locally tailored optical gradients generated by a digital micromirror device (DMD), providing parallel spin selectivity across the array. This approach enables the initialization of programmable spin-charge configurations with controlled defects, including classical antiferromagnetic patterns [Fig. 1(c)]. We probe these on-demand product states with a single-exposure imaging scheme that resolves both spin and density within 20 μs by scattering on stretched states, extending the scheme from [23] (also see Ref. [24]). Fast internal-state control is achieved through radio-frequency (RF) and microwave (MW) antennas that deliver the highest reported Rabi rates on the relevant transitions [25]. These capabilities also position ^{6}Li as a promising candidate for fermionic quantum computation.

*Contact author: philipp.preiss@mpq.mpg.de

Published by the American Physical Society under the terms of the Creative Commons Attribution 4.0 International license. Further distribution of this work must maintain attribution to the author(s) and the published article's title, journal citation, and DOI. Open access publication funded by the Max Planck Society.

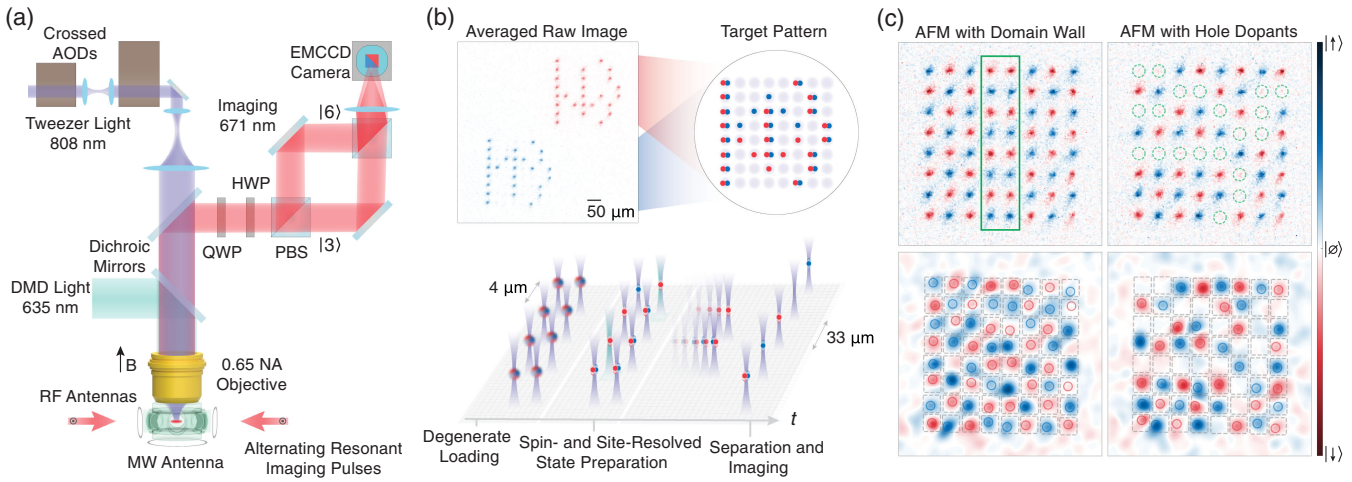


FIG. 1. Arbitrary product state preparation and high-fidelity detection of fermionic atoms. (a) Schematic of the setup. A high-numerical aperture (NA) objective creates 2D tweezer arrays via orthogonal AODs, with superimposed DMD potentials, while collecting 671 nm fluorescence for detection. Spin information is encoded in orthogonally polarized fluorescence photons and separated via polarization optics onto distinct EMCCD regions. (b) Simultaneous spin detection of ^{6}Li ($|3\rangle$: red, $|6\rangle$: blue), shown in an averaged raw image. Example pattern demonstrates arbitrary product state preparation on an 8×8 array; target pattern is shown on the right. The lower panel highlights the programmability of our platform using tweezers (purple) and DMD potentials (green, meshed grid). (c) Representative assembled states for Hubbard physics with overlapped spin sectors. Left: classical antiferromagnet (AFM) with a vertical domain wall (green). Right: hole-doped AFM. Top: averaged raw images; bottom: processed single-shot realizations, in arrays loaded at 4 μm, and imaged at 33 μm separation.

Together, these advances enable programmable, low-entropy initial states with intrinsic fermionic statistics, granting access to computationally challenging many-body physics and emerging architectures for fermionic quantum processing [26–28]. Combined with dynamics in lattices or tunnel-coupled tweezers, they open new opportunities for exploring strongly correlated phases and nonequilibrium behavior. The ability to assemble large product states atom by atom further facilitates protocols that require structured input states, such as Hamiltonian learning, as well as studies of precisely controlled impurity-, disorder-, and frustration-induced phenomena [29,30].

Fast spin-resolved imaging—We begin by introducing a spin- and density-resolved detection scheme, essential for probing state preparation in atomic arrays. For ^{6}Li, spin-resolved imaging is challenging due to its low mass and small fine and hyperfine constants. Existing approaches often rely on mapping internal states onto auxiliary external atomic degrees of freedom, and typically require deep pinning lattices with long (hundreds of ms) exposures [21,31–33]. Building on the free-space approach of [23], we instead obtain spin-resolution with single-atom sensitivity in a single μs-scale exposure by encoding the spin information in the fluorescence polarization, adopting the strategy from [24]. We resonantly drive closed $D2$ ($\sigma^{\pm}$) transitions from the stretched states $|6\rangle$ and $|3\rangle$, to which the science states ($|1\rangle$ and $|2\rangle$) are transferred before detection. At 527 G, these lines are split by 1.46 GHz, resulting in negligible off-resonant scattering. Using polarizing beam splitters in the imaging path, the collected fluorescence from the two orthogonal polarizations is directed onto distinct regions of an electron-multiplying charge-coupled device (EMCCD) camera, separated by ≈ 4.7 mm [Fig. 2(a)]. The key advantage of this method is that a single imaging pulse with two frequency components creates spatially separated images of the two atomic spin states without inherent loss of fluorescence photons.

Figure 2(a) shows the spin-resolved image and histograms obtained for an 8×8 tweezer array loaded with at most one particle per site and spin state. A 19 μs exposure yields ≈ 35 detected photons per atom, resulting in an imaging fidelity above 99.4%. The complete detection sequence, including internal state transfers, realizes a total detection fidelity exceeding 98.5% for both spins [34]. We implement state mappings within 15 μs at 527 G. The $|2\rangle$–$|3\rangle$ transition is driven by a printed circuit board-based RF antenna, which achieves 99.6(5)% fidelity over a 7 μs π pulse [Fig. 2(c)]. For the $|1\rangle$–$|6\rangle$ transition, we employ a single-loop MW antenna with an optimized wideband, uniform rate, smooth truncation (WURST) pulse [43] to provide robustness against magnetic field noise. Although slow field drifts limit multipulse fidelity to ≈ 98%, a single 15 μs optimized π pulse achieves 99.03(5)% transfer fidelity [34]. Additionally, we observe that $|3\rangle$–$|6\rangle$ atoms confined to the same site undergo rapid loss on a few-ms timescale due to spin-changing collisions. To suppress this, the tweezers are switched off prior to state transfers, followed immediately by the imaging pulses. This protocol enables the single-exposure, spin-resolved readout of the tweezer array.

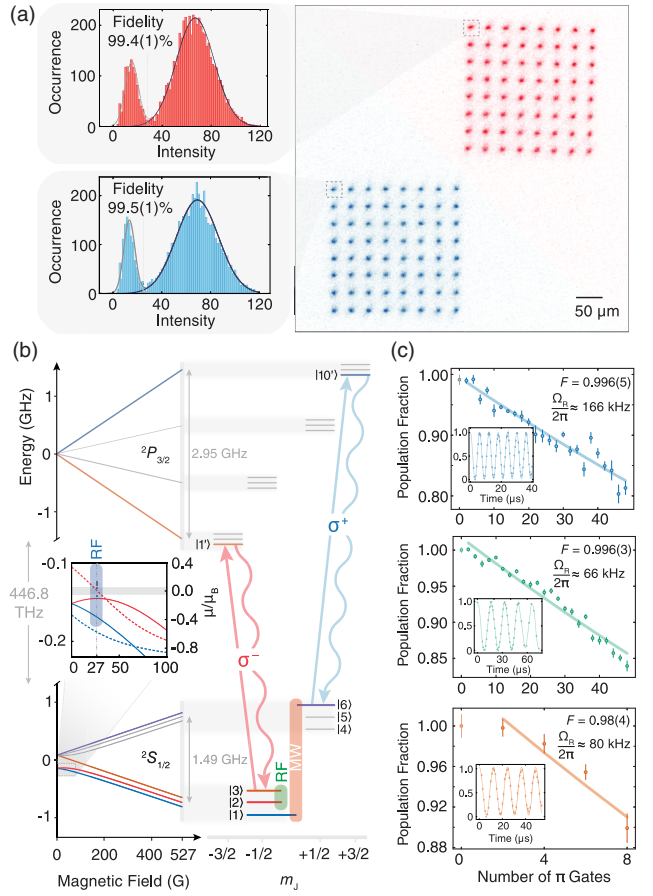


FIG. 2. Rapid single-exposure quantum state readout of ^{6}Li. (a) Averaged single-exposure image of a fully filled array with representative histograms demonstrating high-fidelity 0-1 atom discrimination for both spins. (b) The addressed cycling $D2$ transitions, $|6\rangle \rightarrow |10'\rangle$ and $|3\rangle \rightarrow |1'\rangle$ enable spin-resolved detection. Zeeman energies (solid) and magnetic moments μ (inset, dashed) for $|1\rangle$ (blue) and $|2\rangle$ (red), leveraged for state-dependent potentials. Shaded bands denote the RF and MW antenna-driven transitions. (c) Repeated π-pulse fidelity (F) for the state transfers: $|1\rangle$–$|2\rangle$ (24.3 MHz, blue) for spin-resolved preparation at 27 G, $|2\rangle$–$|3\rangle$ (84.6 MHz, green), and $|1\rangle$–$|6\rangle$ (1.64 GHz, orange) utilized for detection at 527 G. Insets show the measured coherent oscillations with Rabi frequency Ω_R.

Singlet preparation in programmable tweezer arrays—Our approach to initialization of low-entropy fermionic product states begins with preparing a uniform ensemble of ground-state $|1\rangle$–$|2\rangle$ singlet pairs in an optical tweezer array, which serve as a starting point toward engineering structured spin-charge patterns. As shown in Fig. 1(a), an 8×8 array of optical tweezers [$\lambda_T = 808$ nm, waist $= 560(30)$ nm] is generated using orthogonal acousto-optic deflectors (AODs), providing continuous 2D positioning and depth control via multitone RF signals [34]. Ground-state loading exploits Pauli suppression of density fluctuations at the bottom of a Fermi sea, as pioneered in [10]. To ensure this, we create degenerate samples using exponential enhancement of phase-space density through

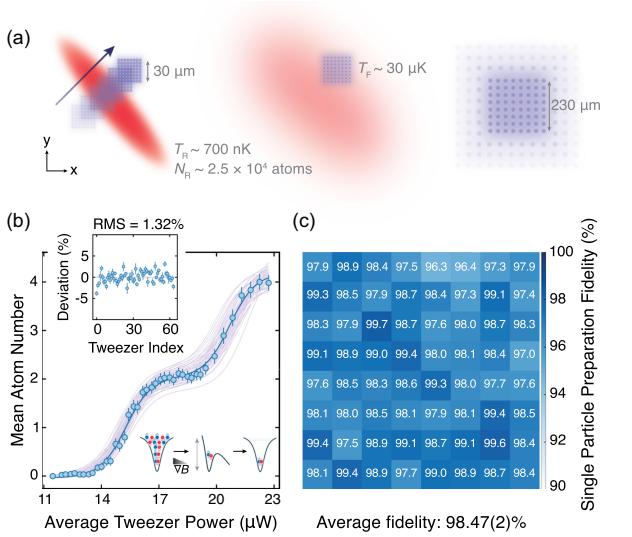


FIG. 3. Deterministic singlet preparation in tweezer arrays. (a) Homogeneous loading is achieved in the tweezer array by translating it across a cold $|1\rangle$–$|2\rangle$ reservoir formed by a 1070 nm ODT. Site occupations are detected after array expansion. (b) Typical spilling curves at $\nabla B = 21.5$ G/cm for individual tweezers (light lines) closely follow the array-average trend (dark line), demonstrating power uniformity (inset). The even-atom plateaus characterize strong two-component Fermi degeneracy. The schematic illustrates selective removal of excited motional states via spilling. (c) Heatmap depicting single-particle preparation fidelities for individual tweezers across the 8×8 array with best tweezers reaching 99.7%.

adiabatic overlap of traps with large volume ratios [44]. A crossed optical dipole trap (ODT) containing an attractively interacting $|1\rangle$–$|2\rangle$ mixture at $T_R \lesssim 700$ nK serves as a reservoir for loading tweezers at 50 μK $\times k_B$ depth and ≈ 4 μm spacing to ensure independent loading [Fig. 3(a)]. The tweezer-trapped sample ($T_F \approx 30$ μK) thermalizes with the reservoir, yielding high degeneracy $T_R/T_F \approx 0.025$ and thus near-unity ground state filling. For arrays sizes comparable to the reservoir, spatial variations in the energy difference between tweezer depth and the reservoir chemical potential lead to inhomogeneous loading. We mitigate this by translating the entire array across the ODT over 50–100 ms at ≈ 0.4 μm/ms, allowing thermalization near the reservoir center, while avoiding rethermalization at the edges. This results in uniform loading of tens of atoms per trap, and scales to larger arrays, with current limits set by imaging constraints. This approach opens up prospects of in-sequence Fermi gas replenishment using separate tweezer arrays for system and reservoir.

From degenerate samples, we create independent singlet pairs by tuning the magnetic field offset to 527 G, where the $|1\rangle$–$|2\rangle$ mixture is effectively noninteracting, and both states have magnetic moments $\approx -\mu_B$ (Bohr magneton). Applying a field gradient with controlled reduction of tweezer depths, we selectively retain only the lowest bound states [10] [Fig. 3(b)]. The trap depths are ramped globally

by stabilizing the laser power before the AODs, using Blackman-shaped pulses to suppress motional excitations. Depth homogeneity is achieved by iteratively tuning the $2N$ RF-tone amplitudes using atomic feedback, exploiting the steep power sensitivity between the zero- and two-atom plateaus in individual spilling curves [21] (see Fig. 3). The resulting $< 1.4\%$ depth variation ensures uniform spilling across the 8×8 array, with the operating point chosen such that residual imperfections manifest predominantly as an atom loss rather than overfilling, verified via atom-resolved counting in a magneto-optical trap [10,34,45]. We benchmark preparation fidelity by performing an additional spill after the sequence to remove any atoms in motional excited states, directly probing the 3D ground-state population [34]. The single-particle ground-state fidelity averages 98.47(2)%, reaching 99.7(0.3:0.4)% in the best tweezers, with ground-state lifetimes of 17.5(1.0) s. Using balanced 2D arrays, we also realize magnetic-gradient-free singlet preparation relying solely on gravity, and achieve similar array-averaged fidelities [$\approx 98.7(1)\%$], demonstrating the applicability of this approach to fermions with negligible magnetic moment [34]. For experimental brevity, we use gradient-assisted spilling for all measurements presented here. These fidelities compare well to the state-of-the-art neutral-atom platforms employing in-trap cooling schemes [9,22,46,47]. Such initialization establishes the singlet array as a uniform, low-entropy baseline for programmable fermionic assembly.

Parallelized spin-dependent preparation—The generation of arbitrary product states further requires precise local spin control. In ^{6}Li, this is complicated by the small fine structure splitting ($\approx$ 10 GHz), which limits optical selectivity by inducing strong off-resonant scattering [48]. Instead, we harness the tunable magnetic moments of the internal states to realize lossless, spin-selective potentials [10]. In particular, at 27 G, $|2\rangle$ exhibits a vanishing magnetic moment, while $|1\rangle$ retains $\mu_{|1\rangle} \approx -0.6\mu_B$ [see Fig. 2(b)]. In a magnetic field gradient, this differential moment yields a spin-dependent potential slope, allowing selective spilling of $|1\rangle$ atoms while leaving $|2\rangle$ unperturbed [49]. We demonstrate this concept by performing a global spin-selective spill on an 8×8 array of $|1\rangle$–$|2\rangle$ singlet pairs [Fig. 4(b)]. The measured ground-state survival probabilities show sharply separated extinction curves

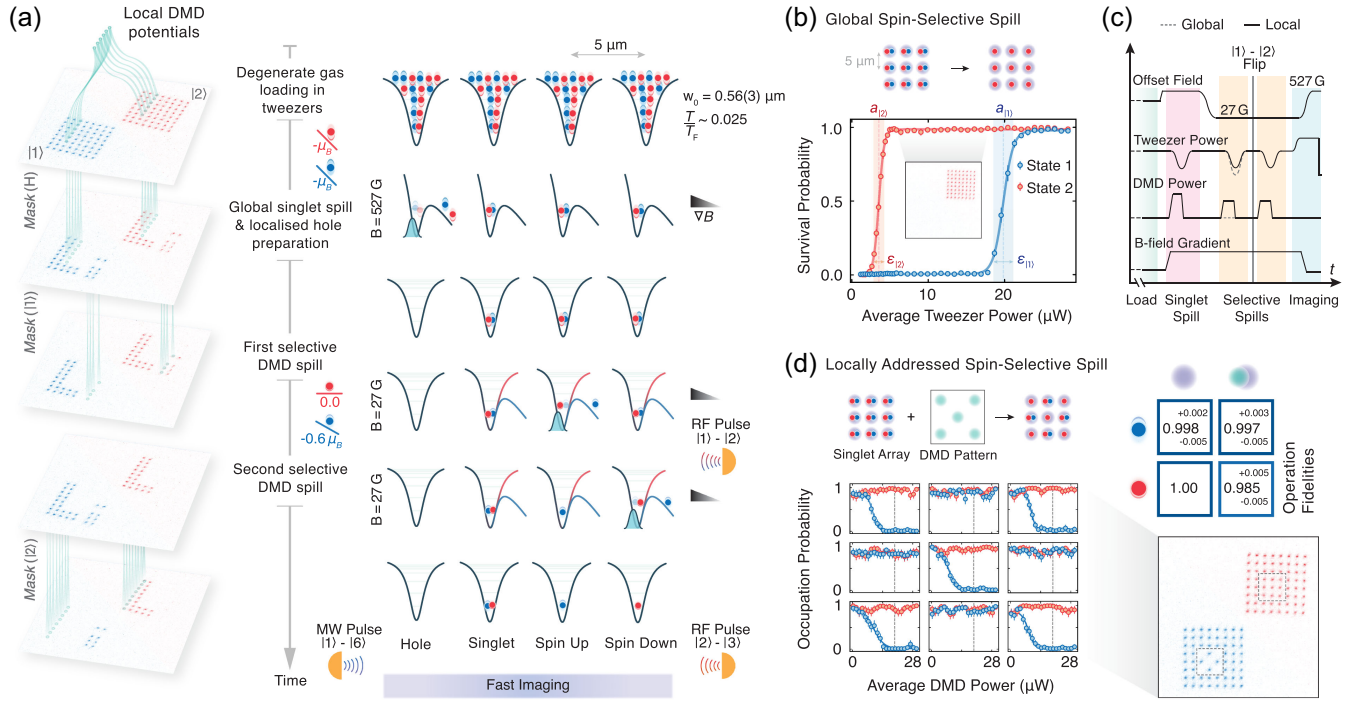


FIG. 4. Arbitrary product state preparation. (a) Schematic of the protocol for preparing a $|2\rangle$–$|1\rangle$ spin-patterned "*L-i*." Left: representative DMD potentials (showing only the first addressed column for clarity; green) with spin-resolved images. Right: axial potential schematic summarizing the concept. First, a global, spin-agnostic spill removes excited motional states, while a repulsive DMD mask, *Mask* (H), simultaneously creates site-resolved holes. A second DMD pattern *Mask* ($|1\rangle$) targets sites designated for $|1\rangle$ occupation, followed by a $|1\rangle$–$|2\rangle$ population swap, and a final pattern *Mask* ($|2\rangle$) that imprints the complementary spin structure, realizing arbitrary spin-charge configurations. (b) Measured spin-selective survival probabilities at fixed $\nabla B = 50$ G/cm. Sigmoid fits yield centers $a_{|1\rangle} = 19.83(3)$ μW, $a_{|2\rangle} = 3.54(2)$ μW, and widths $\varepsilon_{|1\rangle} = 1.30(6)$ μW, $\varepsilon_{|2\rangle} = 0.70(2)$ μW. (c) Experimental sequence mapping key parameters. (d) Local spin-selective spilling using the DMD at fixed tweezer power ($\approx$ 16 μW) and $\nabla B = 21.5$ G/cm. Operational fidelities correspond to the probability of retaining (removing) a specific spin at addressed (nonaddressed) sites in the 3D ground state, evaluated at DMD power marked by the dashed line.

for the two spins, corresponding to a sixfold difference in tweezer depths for the bound state thresholds. We emphasize that this magnetically induced selectivity is very robust and does not rely on the fine-tuned tweezer depths required for singlet preparation.

Building on this, we realize site-resolved control using programmable optical potentials projected by a DMD. Spatially incoherent 635 nm light is used to generate localized repulsive disks with a radius of ≈ 500 nm, aligned to individual tweezers with < 130 nm error. By offsetting the DMD focal plane by a few micrometers, we impose controllable axial gradients on each tweezer. For typical tweezer spilling depths of ≈ 85 kHz, the DMD can apply site-specific potentials of ≈ 500 kHz at its focus—corresponding to optical gradients of ≈ 100 kHz/μm on the atoms. Gray scaling over ≈ 113 mirrors per site provides $\approx 1\%$ depth resolution, and hence of optical gradients. Crucially, the DMD-generated addressing patterns enable independent control over the effective depth of each tweezer, resulting in fully parallelized local control.

In the experiment, following singlet preparation, spin-selective atom removal is performed by combining a magnetic-field gradient, a global tweezer power ramp, and DMD-defined local potentials. The gradient weakens the effective confinement only for $|1\rangle$ atoms, whereas gradient-insensitive $|2\rangle$ atoms remain stably trapped [Fig. 4(a)]. A localized, spin-independent DMD-induced optical gradient on selected sites then nudges only the $|1\rangle$ atoms across the bound-state threshold, leading to their clean removal. In a representative "cross" pattern [Fig. 4(d)], addressed tweezers show 99.7(0.3:0.5)% removal fidelity for $|1\rangle$ and 98.5(0.5:0.5)% probability for $|2\rangle$ retention in the ground state. Nonaddressed sites retain $|1\rangle$ atoms with 99.8(0.2:0.5)% probability and show no detectable change in $|2\rangle$, compared to the initial ground-state sample.

Equipped with site-resolved spin selectivity, we realize arbitrary product states in the 8×8 array (Fig. 1). As outlined in Fig. 4(a), our protocol first employs a DMD mask [*Mask* (H)] that defines the hole pattern during a spin-agnostic global spill, followed by a low-field spin-selective removal with *Mask* ($|1\rangle$) to define the $|1\rangle$ sector. A 3.5 μs RF π pulse then swaps the $|1\rangle$–$|2\rangle$ populations [34], enabling a second selective spill to imprint the $|2\rangle$ pattern via *Mask* ($|2\rangle$). This procedure grants deterministic access to the full local basis—$|\varnothing\rangle$, $|\uparrow\rangle$, $|\downarrow\rangle$, $|\uparrow\downarrow\rangle$, enabling direct atom-by-atom construction of quantum states. The local and parallelized initialization of spin and density in the absence of spin-dependent optical potentials is the main result of this Letter. We demonstrate this control by preparing classical antiferromagnetic ordered states relevant for Fermi-Hubbard physics with engineered domain walls and precisely embedded defects [Fig. 1(c)]. Our approach provides a highly programmable alternative for fermionic state preparation compared to the realization of band insulators and configurational derivatives thereof [11,21,50]. The scheme benefits from the parallelized nature of deterministic local control, achieving arbitrary configurations in at most two spills. For the array sizes explored here, we observe no degradation in entropy per particle or ground-state fraction with increasing system size, consistent with the local character of the preparation stages and indicating the feasibility of larger arrays generated via AODs or spatial light modulators.

In conclusion, we have demonstrated a novel approach for realizing arbitrary product states of fermions in optical tweezer arrays, utilizing spin-resolved deterministic preparation of ^{6}Li atoms in the 3D motional ground state. These results establish microscopic control over the initial quantum state and enable quantum dynamical studies starting from programmable, low-entropy configurations of fermions. We showcase these capabilities by engineering target states of up to 128 atoms, within experimental cycle times of 3 s. For instance, a band-insulator-like pattern is realized on our platform with a $> 14\%$ success probability, corresponding to an average loading entropy of $0.080(1)\ k_B$ per particle. Looking ahead, tunnel coupling such states in the tweezers or via transfer to optical lattices will enable the exploration of Fermi-Hubbard physics seeded with tailored features, such as hole pairs or spin-domain walls. At system sizes of 8×8, these characteristics place our platform in a regime comparable to that of quantum gas microscopes observing strong correlation phenomena at low temperatures [51], as well as to state-of-the-art experiments studying far-from-equilibrium dynamics [52,53]. They also match the system sizes accessible to leading numerical methods investigating charge and spin ordering in doped Hubbard systems [54,55]. The array size in our implementation is limited by the diffusion dynamics during free-space fluorescence and the associated requirement for array expansion before imaging. Overcoming this limitation by techniques such as matter-wave magnification [56,57] provides a direct route to scaling to larger system sizes. The preparation via singlets is compatible with further cooling via entropy redistribution [11] and post-selection into the zero-magnetization sector [21]. More broadly, the capability to initialize fermionic quantum states with programmable spin composition offers a direct route to itinerant ferromagnetism and Fulde-Ferrell-Larkin-Ovchinnikov physics in spin-imbalanced systems [58,59].

Acknowledgments—We thank the Heidelberg Quantum Architecture team at Heidelberg University for the initial development and continued collaboration on the modular quantum gas platform. We are grateful for helpful exchanges with the Lithium quantum gas microscope team and the FermiQP team at MPQ and thank Gaurav Vaidya, Cady Feng, Daniel Dux, Jonas Kruip, Xinyi Huang, Kirill Khoruzhii, Jun Ong, and Pragya Sharma, along with Anton Mayer and Milan Antic, for their support during the initial

stages and construction of the apparatus. We thank Adam Kaufman and Petar Bojović for a careful reading of the manuscript. This work was supported by the Max Planck Society, the European Union's Horizon 2020 and Horizon Europe research and innovation programs (Grant Agreements No. 948240—ERC Starting Grant UniRand—and No. 101212809—ERC Proof of Concept FermiChem) and Germany's Excellence Strategy (EXC-2111-390814868).

Data availability—The data that support the findings of this article are not publicly available. The data are available from the authors upon reasonable request.

[1] I. M. Georgescu, S. Ashhab, and F. Nori, Quantum simulation, Rev. Mod. Phys. **86**, 153 (2014).
[2] M. Saffman, T. G. Walker, and K. Mølmer, Quantum information with Rydberg atoms, Rev. Mod. Phys. **82**, 2313 (2010).
[3] A. D. Ludlow, M. M. Boyd, J. Ye, E. Peik, and P. O. Schmidt, Optical atomic clocks, Rev. Mod. Phys. **87**, 637 (2015).
[4] C. Gross and I. Bloch, Quantum simulations with ultracold atoms in optical lattices, Science **357**, 995 (2017).
[5] L. Henriet, L. Beguin, A. Signoles, T. Lahaye, A. Browaeys, G.-O. Reymond, and C. Jurczak, Quantum computing with neutral atoms, Quantum **4**, 327 (2020).
[6] W. S. Bakr, Z. Ba, and M. L. Prichard, Microscopy of ultracold fermions in optical lattices, arXiv:2507.04042v1.
[7] B. J. Lester, N. Luick, A. M. Kaufman, C. M. Reynolds, and C. A. Regal, Rapid production of uniformly filled arrays of neutral atoms, Phys. Rev. Lett. **115**, 073003 (2015).
[8] D. Bluvstein *et al.*, Logical quantum processor based on reconfigurable atom arrays, Nature (London) **626**, 58 (2024).
[9] R. M. Kroeze, R. A. Villela, E. Zu, T. O. Höhn, and M. Aidelsburger, Isotope-agnostic motional ground-state cooling of neutral Yb atoms, Phys. Rev. Res. **7**, L042061 (2025).
[10] F. Serwane, G. Zürn, T. Lompe, T. B. Ottenstein, A. N. Wenz, and S. Jochim, Deterministic preparation of a tunable few-fermion system, Science **332**, 336 (2011).
[11] M. Xu, L. H. Kendrick, A. Kale, Y. Gang, C. Feng, S. Zhang, A. W. Young, M. Lebrat, and M. Greiner, A neutral-atom Hubbard quantum simulator in the cryogenic regime, Nature (London) **642**, 909 (2025).
[12] J. Eisert, M. Friesdorf, and C. Gogolin, Quantum many-body systems out of equilibrium, Nat. Phys. **11**, 124 (2015).
[13] A. Mitra, Quantum quench dynamics, Annu. Rev. Condens. Matter Phys. **9**, 245 (2018).
[14] S. Moudgalya, B. A. Bernevig, and N. Regnault, Quantum many-body scars and Hilbert space fragmentation: A review of exact results, Rep. Prog. Phys. **85**, 086501 (2022).
[15] T. A. Hilker, G. Salomon, F. Grusdt, A. Omran, M. Boll, E. Demler, I. Bloch, and C. Gross, Revealing hidden antiferromagnetic correlations in doped Hubbard chains via string correlators, Science **357**, 484 (2017).
[16] L. H. Kendrick, A. Kale, Y. Gang, A. D. Deters, M. Lebrat, A. W. Young, and M. Greiner, Pseudogap in a Fermi-Hubbard quantum simulator, arXiv:2509.18075.
[17] T. Hartke, B. Oreg, C. Turnbaugh, N. Jia, and M. Zwierlein, Direct observation of nonlocal fermion pairing in an attractive Fermi-Hubbard gas, Science **381**, 82 (2023).
[18] C. Gross and W. S. Bakr, Quantum gas microscopy for single atom and spin detection, Nat. Phys. **17**, 1316 (2021).
[19] M. C. Tichy, M. Tiersch, F. Mintert, and A. Buchleitner, Many-particle interference beyond many-Boson and many-fermion statistics, New J. Phys. **14**, 093015 (2012).
[20] P. Lunt, P. Hill, J. Reiter, P. M. Preiss, M. Gałka, and S. Jochim, Realization of a Laughlin state of two rapidly rotating fermions, Phys. Rev. Lett. **133**, 253401 (2024).
[21] Z. Z. Yan, B. M. Spar, M. L. Prichard, S. Chi, H.-T. Wei, E. Ibarra-García-Padilla, Kaden R. A. Hazzard, and W. S. Bakr, Two-dimensional programmable tweezer arrays of fermions, Phys. Rev. Lett. **129**, 123201 (2022).
[22] A. W. Young, W. J. Eckner, N. Schine, A. M. Childs, and A. M. Kaufman, Tweezer-programmable 2D quantum walks in a Hubbard-regime lattice, Science **377**, 885 (2022).
[23] A. Bergschneider, V. M. Klinkhamer, J. H. Becher, R. Klemt, G. Zürn, P. M. Preiss, and S. Jochim, Spin-resolved single-atom imaging of ^{6}Li in free space, Phys. Rev. A **97**, 063613 (2018).
[24] T. Hammel, M. Kaiser, D. Dux, M. Weidemüller, and S. Jochim, Atom and spin resolved imaging in a single shot, arXiv:2512.09865.
[25] F. Scazza, G. Del Pace, L. Pieri, R. Concas, W. J. Kwon, and G. Roati, A low-impedance radio-frequency circuit for fast spin manipulations in cold alkali atoms, Rev. Sci. Instrum. **96**, 104713 (2025).
[26] D. González-Cuadra, D. Bluvstein, M. Kalinowski, R. Kaubruegger, N. Maskara, P. Naldesi, T. V. Zache, A. M. Kaufman, M. D. Lukin, H. Pichler, B. Vermersch, J. Ye, and P. Zoller, Fermionic quantum processing with programmable neutral atom arrays, Proc. Natl. Acad. Sci. U.S.A. **120**, e2304294120 (2023).
[27] R. Ott, D. González-Cuadra, T. V. Zache, P. Zoller, A. M. Kaufman, and H. Pichler, Error-corrected fermionic quantum processors with neutral atoms, Phys. Rev. Lett. **135**, 090601 (2025).
[28] A. Schuckert, E. Crane, A. V. Gorshkov, M. Hafezi, and M. J. Gullans, Fault-tolerant fermionic quantum computing, arXiv:2411.08955.
[29] A. Dutkiewicz, T. E. O'Brien, and T. Schuster, The advantage of quantum control in many-body Hamiltonian learning, Quantum **8**, 1537 (2024).
[30] P. Massignan, M. Zaccanti, and G. M. Bruun, Polarons, dressed molecules and itinerant ferromagnetism in ultracold Fermi gases, Rep. Prog. Phys. **77**, 034401 (2014).
[31] P. M. Preiss, R. Ma, M. E. Tai, J. Simon, and M. Greiner, Quantum gas microscopy with spin, atom-number, and multilayer readout, Phys. Rev. A **91**, 041602(R) (2015).
[32] M. Boll, T. A. Hilker, G. Salomon, A. Omran, J. Nespolo, L. Pollet, I. Bloch, and C. Gross, Spin- and density-resolved microscopy of antiferromagnetic correlations in Fermi-Hubbard chains, Science **353**, 1257 (2016).
[33] L. W. Cheuk, M. A. Nichols, K. R. Lawrence, M. Okan, H. Zhang, E. Khatami, N. Trivedi, T. Paiva, M. Rigol, and

M. W. Zwierlein, Observation of spatial charge and spin correlations in the 2D Fermi-Hubbard model, Science **353**, 1260 (2016).

[34] See Supplemental Material at http://link.aps.org/supplemental/10.1103/fsmh-dz71 for details of the experimental setup, technical information on the antennas, and discussions on image processing, calibration measurements, and entropy calculations, which includes Refs. [35–42].

[35] T. G. Tiecke, S. D. Gensemer, A. Ludewig, and J. T. M. Walraven, High-flux two-dimensional magneto-optical-trap source for cold lithium atoms, Phys. Rev. A **80**, 013409 (2009).

[36] T. Hammel, M. Kaiser, D. Dux, P. M. Preiss, M. Weidemüller, and S. Jochim, Modular quantum gas platform, Phys. Rev. A **111**, 033314 (2025).

[37] M. Schroeder, Synthesis of low-peak-factor signals and binary sequences with low autocorrelation (corresp.), IEEE Trans. Inf. Theory **16**, 85 (1970).

[38] R. Grimm, M. Weidemüller, and Y. B. Ovchinnikov, Optical dipole traps for neutral atoms, Adv. At. Mol. Opt. Phys. **42**, 95 (2000).

[39] E. Torrontegui, S. Ibáñez, X. Chen, A. Ruschhaupt, D. Guéry-Odelin, and J. G. Muga, Fast atomic transport without vibrational heating, Phys. Rev. A **83**, 013415 (2011).

[40] A. C. Gossard, V. Jaccarino, and J. H. Wernick, Ytterbium NMR:Yb^{171} nuclear moment and Yb metal knight shift, Phys. Rev. **133**, A881 (1964).

[41] L. Su, A. Douglas, M. Szurek, A. H. Hébert, A. Krahn, R. Groth, G. A. Phelps, O. Marković, and M. Greiner, Fast single atom imaging for optical lattice arrays, Nat. Commun. **16**, 1017 (2025).

[42] B. M. Spar, E. Guardado-Sanchez, S. Chi, Z. Z. Yan, and W. S. Bakr, Realization of a Fermi-Hubbard optical tweezer array, Phys. Rev. Lett. **128**, 223202 (2022).

[43] O. C. Andronesi, S. Ramadan, E.-M. Ratai, D. Jennings, C. E. Mountford, and A. G. Sorensen, Spectroscopic imaging with improved gradient modulated constant adiabaticity pulses on high-field clinical scanners, J. Magn. Reson. **203**, 283 (2010).

[44] D. M. Stamper-Kurn, H.-J. Miesner, A. P. Chikkatur, S. Inouye, J. Stenger, and W. Ketterle, Reversible formation of a Bose-Einstein condensate, Phys. Rev. Lett. **81**, 2194 (1998).

[45] D. B. Hume, I. Stroescu, M. Joos, W. Muessel, H. Strobel, and M. K. Oberthaler, Accurate atom counting in mesoscopic ensembles, Phys. Rev. Lett. **111**, 253001 (2013).

[46] A. M. Kaufman, B. J. Lester, and C. A. Regal, Cooling a single atom in an optical tweezer to its quantum ground state, Phys. Rev. X **2**, 041014 (2012).

[47] A. Jenkins, J. W. Lis, A. Senoo, W. F. McGrew, and A. M. Kaufman, Ytterbium nuclear-spin qubits in an optical tweezer array, Phys. Rev. X **12**, 021027 (2022).

[48] M. Lebrat, S. Häusler, P. Fabritius, D. Husmann, L. Corman, and T. Esslinger, Quantized conductance through a spin-selective atomic point contact, Phys. Rev. Lett. **123**, 193605 (2019).

[49] A. N. Wenz, G. Zürn, S. Murmann, I. Brouzos, T. Lompe, and S. Jochim, From few to many: Observing the formation of a Fermi sea one atom at a time, Science **342**, 457 (2013).

[50] P. Sompet, S. Hirthe, D. Bourgund, T. Chalopin, J. Bibo, J. Koepsell, P. Bojović, R. Verresen, F. Pollmann, G. Salomon, C. Gross, T. A. Hilker, and I. Bloch, Realizing the symmetry-protected Haldane phase in Fermi-Hubbard ladders, Nature (London) **606**, 484 (2022).

[51] A. Bohrdt, L. Homeier, C. Reinmoser, E. Demler, and F. Grusdt, Exploration of doped quantum magnets with ultracold atoms, Ann. Phys. (Amsterdam) **435**, 168651 (2021).

[52] A. L. Shaw, D. K. Mark, J. Choi, R. Finkelstein, P. Scholl, S. Choi, and M. Endres, Experimental signatures of Hilbert-space ergodicity: Universal bitstring distributions and applications in noise learning, Phys. Rev. X **15**, 031001 (2025).

[53] S. Karch, S. Bandyopadhyay, Z.-H. Sun, A. Impertro, S. Huh, I. P. Rodríguez, J. F. Wienand, W. Ketterle, M. Heyl, A. Polkovnikov, I. Bloch, and M. Aidelsburger, Probing quantum many-body dynamics using subsystem Loschmidt echos, arXiv:2501.16995.

[54] T. Blatz, U. Schollwöck, F. Grusdt, and A. Bohrdt, Two-dopant origin of competing stripe and pair formation in Hubbard and $t-J$ models, Phys. Rev. X **15**, 031074 (2025).

[55] J. R. Moreno, G. Carleo, A. Georges, and J. Stokes, Fermionic wave functions from neural-network constrained hidden states, Proc. Natl. Acad. Sci. U.S.A. **119** (2022).

[56] P. A. Murthy, D. Kedar, T. Lompe, M. Neidig, M. G. Ries, A. N. Wenz, G. Zürn, and S. Jochim, Matter-wave Fourier optics with a strongly interacting two-dimensional Fermi gas, Phys. Rev. A **90**, 043611 (2014).

[57] L. Asteria, H. P. Zahn, M. N. Kosch, K. Sengstock, and C. Weitenberg, Quantum gas magnifier for sub-lattice-resolved imaging of 3D quantum systems, Nature (London) **599**, 571 (2021).

[58] S. Pilati, G. Bertaina, S. Giorgini, and M. Troyer, Itinerant ferromagnetism of a repulsive atomic Fermi gas: A quantum Monte Carlo study, Phys. Rev. Lett. **105**, 030405 (2010).

[59] J. J. Kinnunen, J. E. Baarsma, J.-P. Martikainen, and P. Törmä, The Fulde–Ferrell–Larkin–Ovchinnikov state for ultracold fermions in lattice and harmonic potentials: A review, Rep. Prog. Phys. **81**, 046401 (2018).